AMSU-A Antenna Pattern Corrections

Tsan Mo

***Abstract*—A procedure for making antenna pattern corrections to antenna temperatures of the advanced microwave sounding unit-A (AMSU-A) is developed. Antenna efficiencies, fractions of total power over three different solid-angle regions subtended at the satellite by the earth (plus atmosphere below 20 km), cold space, and the satellite platform, were calculated at 30 earth views and four possible cold space calibration positions. These calculated results simplify the process for correcting antenna temperature measurements to retrieve the true brightness temperatures from AMSU-A data. Using the antenna pattern data and a profile of atmospheric brightness temperature, a set of antenna pattern corrections was simulated for each channel at the 30 earth views and four possible cold space calibration positions. The results show that these corrections can add 0.5 to 2.7 K to the antenna temperatures to retrieve the brightness temperatures and that the cold space calibration temperatures may be raised to 2 K above the nominal cold sky temperature of 2.73 K. Antenna pattern 3-dB beamwidths and main-beam efficiencies were also calculated from the antenna pattern data.**

***Index Terms*—Antenna measurements, antenna radiation patterns, microwave antenna, microwave radiometry, remote sensing, satellite applications, temperature sounding.**

I. Introduction

STARTING in 1998, the NOAA will launch a new generation of total-power microwave radiometers, AMSU-A, on its NOAA-K, L, M, and N series of polar-orbiting operational environmental satellites (POES). Each AMSU-A instrument is composed of two separate units: AMSU-A2 with two channels at 23.8 and 31.4 GHz and AMSU-A1 with 12 channels in the range of 50.3–57.3 GHz and one channel at 89.0 GHz. Totally, AMSU-A furnishes 15 channels. A description of the AMSU-A instrument and its radiometric performance was reported elsewhere [1]. In tandem with each AMSU-A, there will be also an AMSU-B, which has five channels with frequencies at 89 and 150 GHz and three channels around the 183-GHz water vapor line. AMSU-B, which is provided by the United Kingdom Meteorological Office, is for humidity sounding and has been described in [2]. Only a brief description of the AMSU-A instruments is given here.

AMSU-A1 uses two antenna systems, providing a set of the 12 oxygen band channels (3–14) for retrieving the atmospheric temperature profile from the earth's surface to about 42 km, or from 1000–2 mb. The remaining three channels (1 and 2 from A2 and 15 from A1) will aid in the retrieval of temperature soundings by correction of surface emissivity, atmospheric liquid water, and total precipitable water. These window channels also provide information on precipitation, sea ice, and snow coverage.

Table I lists some of the main AMSU-A channel characteristics, which include the channel frequency, number of bands, bandwidth, and radiometric temperature sensitivity (or NEΔT) for each channel. Details of these quantities are given in [1], and the beam efficiency and beamwidth (both correspond to beam position 15) will be discussed in Section IV of this study. Each antenna system consists of an offset parabolic reflector housed in a cylindrical shroud. The reflectors rotate one complete revolution every 8 s, during which 30 earth scenes (also referred to as beam positions, within 48°20′ from nadir and each separated by 3°20′) will be sampled in a stepped-scan fashion. Onboard calibration is performed every 8 s by viewing an internal blackbody target (at 180° from nadir) and the cold space in one of four possible viewing positions located between -76 and -84° from nadir. Beam positions 1 and 30 are the extreme scan positions of the earth views, while beam positions 15 and 16 are at 1°40′ and -1°40′ from the nadir direction, respectively.

Measurements of the antenna pattern is an important part of the AMSU-A calibration process. AMSU-A specification requires that the antenna beamwidth at half-maximum points (3-dB width) should be 3.3° $\pm$ 10% and that the main beam efficiency, which is defined as the ratio of the power (including both copolarizations and cross polarizations) received by an antenna within its main beam to the total power received from all solid angles, must be $\geq$95%. Here, the main beam is defined as 2.5$\times$ the 3-dB beamwidth. The remaining portion ($\approx$5%) of the total power received by the antenna via its sidelobes originates from a wide angular range that includes the satellite platform and cold space (sky), where the cosmic background brightness temperature, 2.73 K, is considerably less than the earth's temperatures. This study was undertaken to develop a procedure for making the antenna pattern sidelobe corrections to the antenna temperatures at 30 earth scenes from the NOAA-K AMSU-A instruments since there is no technical report for antenna pattern corrections at these scenes from the antenna manufacturer. The main beam efficiency and 3-dB beamwidth for each channel were also calculated for comparison with the AMSU-A specifications.

II. Theoretical Development

The antenna pattern corrections and recovery of brightness temperatures from measured antenna temperatures obtained from various satellite-borne radiometers [3]–[6] have been studied previously. We take advantage of these studies and adopt some of their approaches for formulating the procedures in making the antenna pattern corrections for the AMSU-A

Manuscript received December 6, 1996; revised November 5, 1997.

The author is with the Climate Research and Applications Division, Office of Research and Applications, NESDIS/NOAA, Camp Springs, MD 20746 USA.

Publisher Item Identifier S 0196-2892(99)00091-1.

TABLE I
CHANNEL CHARACTERISTICS AND SPECIFICATIONS OF AMSU-A2 PFM AND AMSU-A1 FM1 FOR NOAA-K. THE BEAM EFFICIENCIES AND BEAMWIDTHS CORRESPOND TO BEAM POSITION 15

Channel Number	Channel Frequency		Number of Bands	Measured 3-dB RF Bandwidth (MHz)	NEΔT		Main Beam Efficiency	Cross Polarization Beam Efficiency	3-dB Beamwidth (deg.) **	Polarization at nadir	Remarks
	Specification (MHz)	Measured * (MHz)			Spec. (K)	Measred (K)					
1	23800	23800.37	1	251.02	0.30	0.211	95.39%	1.57%	3.53	V	A2/PFM
2	31400	31400.42	1	161.20	0.30	0.265	97.14%	1.23%	3.41	V	"
3	50300	50299.91	1	161.14	0.40	0.219	95.39%	2.24%	3.76	V	A1-2/FM1
4	52800	52799.39	1	380.52	0.25	0.143	95.50%	1.21%	3.72	V	"
5	53596 ± 115	53595.41 ± 115	2	168.20 I 168.20	0.25	0.148	95.55%	1.38%	3.70	H	"
6	54400	54399.53	1	380.54	0.25	0.154	95.08%	1.65%	3.68	H	A1-1/FM1
7	54940	54940.64	1	380.56	0.25	0.132	94.79%	1.47%	3.61	V	"
8	55500	55498.70	1	310.34	0.25	0.141	95.05%	1.44%	3.63	H	A1-2/FM1
9	fo = 57290.344	fo = 57290.33	1	310.42	0.25	0.236	95.91%	1.29%	3.51	H	A1-1/FM1
10	fo ± 217	fo ± 217	2	76.58 I 76.58	0.40	0.250				H	"
11	fo ± 322.2 ± 48	fo ± 322.2 ± 48	4	34.28 / 35.11 I 35.11 / 34.28	0.40	0.280				H	"
12	fo ± 322.2 ± 22	fo ± 322.2 ± 22	4	15.08 / 15.29 I 15.29 / 15.08	0.60	0.400				H	"
13	fo ± 322.2 ± 10	fo ± 322.2 ± 10	4	7.92 / 7.93 I 7.93 / 7.92	0.80	0.539				H	"
14	fo ± 322.2 ± 4.5	fo ± 322.2 ± 4.5	4	2.94 / 2.92 I 2.92 / 2.94	1.20	0.914				H	"
15	89000	88997.00	1	1998.98	0.50	0.166	97.79%	1.38%	3.80	V	"

* At temperature 18 degree C. ** Specification is required to have 3.3 degrees ± 10% for all channels.

instrument. In this section, the appropriate formulas for calculating the antenna pattern corrections are developed.

A geometric sketch of the scanning AMSU-A antenna on a satellite is given in Fig. 1, where the satellite S is at a height $h = \overline{HS}$ ($h \approx 850$ km for POES) above the earth's surface. A Cartesian coordinate system $x'y'z'$ is placed at the earth's center O. We assume that the y'–z' plane contains the POES's orbit. Without loss of generality, the AMSU-A antenna boresight is assumed to scan crosstrack in the x'–z' plane to acquire data at 30 earth views, cold space, and the blackbody target, respectively. For convenience, a second set of coordinate system xyz, which is parallel to the first set, is attached to the satellite S. Another coordinate system uvw, which is useful in performing integrations involving antenna pattern functions, is obtained by rotating the x–z plane around the y-axis by an angle β (defined below). After this rotation, the w-axis aligns with the negative boresight direction.

Assume that the AMSU-A antenna system looks at the boresight direction B (in the x–z plane), which makes a scan angle β (=∠OSB) with the nadir (or $-z$ axis). Let P denote a general ray pointing at an arbitrary direction defined by $\Omega = (\theta, \phi)$, where θ is the angle ∠OSP measured from the nadir and ϕ is the azimuthal angle measured from the x-axis. Then the measured antenna temperature $T_A(\beta)$ at the scan angle β can be defined as

$$T_A(\beta) = \frac{1}{N} \int_{4\pi} G T_B \, d\Omega \tag{1}$$

where the normalization factor N, which is the total antenna-pattern solid angle, is defined as

$$N = \int_{4\pi} G \, d\Omega. \tag{2}$$

The T_B represents the brightness temperature at the elementary solid angle $d\Omega = \sin\theta \, d\theta \, d\phi$ and is, in general, a function of θ and ϕ, but it can be approximated by $T_B = T_B(\theta, \phi) \approx T_B(\theta)$ for a horizontally homogenous atmospheric layers. The quantity $G = G(\alpha, \gamma)$, which is a function of the angles α and γ in the uvw-coordinate system as defined below, is the antenna pattern function with its central peak being along the boresight direction β. The G consists of both copolarization and cross-polarization components, both of which were measured. It is defined as

$$G(\alpha, \gamma) = G_{\text{co}}(\alpha, \gamma) + G_{\text{cross}}(\alpha, \gamma) \tag{3}$$

where G_{co} and G_{cross} are the measured copolarized and cross-polarized antenna pattern, respectively. Both components are normalized with respect to the boresight maximum of the copolarization data.

It is convenient to perform the integrations in (1) and (2) if G is expressed as a function of the angle α (=∠PSB) from the antenna boresight direction $\vec{B}$ and an "equivalent" azimuthal

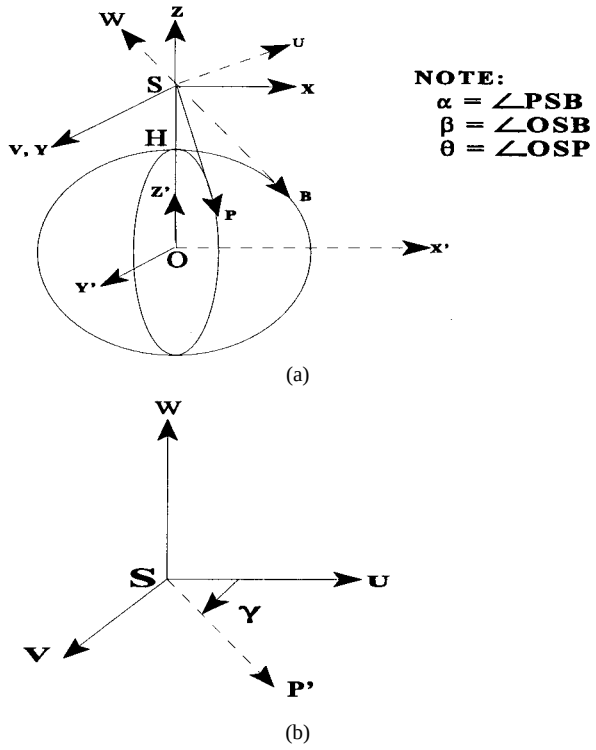

Fig. 1. (a) Geometric sketch of the satellite and earth relationship and (b) define the angle γ in the uvw coordinate system. The SP' is the projection of SP on the u–v plane.

angle γ within the coordinate system uvw. Fig. 1(b) shows the definition of γ, which is the angle between the u-axis and the projection SP' of SP on the u–v plane.

From the geometry in Fig. 1, we can derive the formulas that express α and γ as a function of θ, ϕ, and β. Let $\hat{B}$ represent a unit vector along $\vec{B}$, and let $\vec{P}$ represent a unit vector along $\vec{P}$. Then

$$\hat{B} = \sin\beta\hat{x} - \cos\beta\hat{z} \tag{4}$$

and

$$\hat{P} = \sin\theta\cos\phi\hat{x} + \sin\theta\sin\phi\hat{y} - \cos\theta\hat{z} \tag{5}$$

where the $(\hat{x}, \hat{y}, \hat{z})$ are unit vectors along the (x, y, z) axes. Therefore, the angle α can be determined from the dot product of the two unit vectors and is defined by the relation

$$\alpha = \cos^{-1}(\hat{P}\cdot\hat{B}) = \cos^{-1}(\sin\beta\sin\theta\cos\phi + \cos\beta\cos\theta). \tag{6}$$

Next, we want to express γ as a function of θ, ϕ, and β. Let $(\hat{u}, \hat{v}, \hat{w})$ denote the unit vectors along the (u, v, w) axes. Then the relationship between $(\hat{u}, \hat{v}, \hat{w})$ and $(\hat{x}, \hat{y}, \hat{z})$ is defined by the rotation equations,

$$\begin{aligned}\hat{u} &= \hat{x}\cos\beta + \hat{z}\sin\beta\\ \hat{v} &= \hat{y}\\ \hat{w} &= -\hat{x}\sin\beta + \hat{z}\cos\beta.\end{aligned} \tag{7}$$

The azimuthal angle γ [Fig. 1(b)], which is the angle measured from the u–w plane to the w–p plane within the coordinate system uvw, is defined as

$$\begin{aligned}\gamma &= \tan^{-1}\left(\frac{\hat{P}\cdot\hat{v}}{\hat{P}\cdot\hat{u}}\right)\\ &= \tan^{-1}\left(\frac{\sin\theta\sin\phi}{\cos\beta\sin\theta\cos\phi - \sin\beta\cos\theta}\right)\end{aligned} \tag{8}$$

where (5) and (7) have been used to obtain the two dot products in (8). The α and γ constitute the spherical angles around the boresight direction in the uvw coordinate system. These two angles will be used to determine the G values in the integrations.

At a fixed β, (6) and (8) give a one-to-one correspondence between (α, γ) and (θ, ϕ). We can rewrite (1) as

$$\begin{aligned}T_A(\beta) = \frac{1}{N}\Bigg[&\int_0^{\theta_{\max}} g(\theta)T_E(\theta)\sin\theta\,d\theta + \int_{\theta_{\max}}^{\pi/2} g(\theta)T_C\\ &\cdot\sin\theta\,d\theta + \int_{\pi/2}^{\pi} g(\theta)T_{\text{sat}}\sin\theta\,d\theta\Bigg]\end{aligned} \tag{9}$$

where

$$g(\theta) = \int_0^{2\pi} G(\alpha, \gamma)\,d\phi. \tag{10}$$

The antenna temperature $T_A(\beta)$ in (9) consists of three components that are represented by the three integrals on the right-hand side, where the $T_E(\theta)$, T_C, and T_{sat} denote the brightness temperatures of the earth, cold space, and satellite platform, respectively. The integration limit $\theta_{\max}$ in (9) is the half-cone angle subtended by the earth and the atmosphere below 20 km at the satellite that is at a height of $h \approx 850$ km above the earth's surface. Following previous reports [7], the atmosphere below 20 km is considered as an extended shell of the earth for computing the antenna pattern sidelobe corrections. It can be shown from Fig. 1 that $\theta_{\max}$ is defined by

$$\theta_{\max} = \sin^{-1}\left(\frac{R+20}{R+h}\right) \tag{11}$$

where R is the earth's radius and h is the height of the satellite. This gives $\theta_{\max} = 62.26°$ with $R = 6371.2$ km. The factor $(R+20)$ on the numerator indicates that the half-cone angle is extended beyond the earth's surface to include the atmosphere below 20 km.

Equations (1) and (9) are given in terms of brightness temperatures, but both are still valid if all temperatures are replaced by their corresponding radiances. The conversion between radiance and temperature are via the Planck function. Since the Rayleigh–Jeans approximation breaks down at the cold space temperature (~2.73 K), we make all calculations in radiances, which are then converted into temperatures as the final products.

Equation (9) gives a good representation for simulating the antenna temperature if the brightness temperatures $T_E(\theta)$, T_C, and T_{sat} are known. The last two quantities are approximately constant over the range of individual integrations, but $T_E(\theta)$ may vary considerably over its integration limits. However, the AMSU-A antenna patterns are all sharply peaked and decrease rapidly as the scan angle moves away from the boresight direction. Thus, $T_E(\theta)$ can be approximated by a constant $\overline{T}_E$, which represents a mean atmospheric brightness temperature for each channel in the neighborhood of boresight direction β when it is on the earth views. On the other hand, if the boresight direction is on a space view when the T_A is calculated, the earth contribution comes mainly from the limb, which, in our case, is the atmosphere at 20 km above the earth's surface, where brightness temperature is approximately 210 K. Therefore, $T_E = 210$ K will be used when T_A is calculated at the four space views.

The above discussion assumes all radiation sources are far away from the antenna system (i.e., in the "far field"). However, the satellite platform, which is in the "near field" of the antenna, alters its far-field radiation pattern. Ideally, we should use the far-field patterns measured with a mockup of the satellite platform attached to the antenna. However, such a measurement would be costly if it is not impossible. Computer simulation is an alternative approach, which was performed at one of the cold space calibration positions by the instrument manufacturer. Its result showed that the near-field effect of the satellite platform reduces the contribution [8] from the last integration in (9). To match this computer simulated result of near-field effect, a scale factor η is introduced into the last term in (9). The η values for individual channels will given in Section IV-C. Then it is reasonable to approximate the integrations in (9) as a combination of three products, each of which represents a weighted mean brightness temperature

within its integration region

$$T_A(\beta) = \frac{1}{N_\eta}\left[f_e(\beta)\overline{T}_E + f_c(\beta)\overline{T}_C + \eta f_{\rm sat}(\beta)\overline{T}_{\rm Sat}\right] \quad (12)$$

where N_η is a renormalization factor, which is necessary because of the inclusion of the scale factor η, and it is defined as

$$N_\eta = f_e(\beta) + f_c(\beta) + \eta f_{\rm sat}(\beta). \quad (13)$$

The corresponding antenna efficiencies $f_x(\beta)$, where $x = e$, c, or sat, in (12), are defined by,

$$f_x(\beta) = \frac{1}{N}\int_{\theta_x} g(\theta)\,\sin(\theta)\,d(\theta) \quad (14)$$

where the integration limit θ_x (with $x = e, c,$ or sat) corresponds to the one for earth, cold space, or satellite platform, respectively, as given in (9). The antenna efficiencies $f_x(\beta)$ will be computed at the 30 earth views and four cold calibration positions for all channels, of which antenna pattern data are available. Then, we can compute corrections for both the earth views and cold space views. It should be noted that normalization requires $f_e(\beta)+f_c(\beta)+f_{\rm sat}(\beta) = 1$ for a fixed β value.

In (12), the $\overline{T}_C(=2.73)$ K is the cold space temperature. The $\overline{T}_{\rm Sat}$ represents the total energy emanation associated with the satellite platform and it may consist of satellite-platform radiation as well as reflection of radiations from the earth and cold space. In Section IV-D, we will show that the maximum contribution from the last term in (12) is in an order of 0.01 K, which is negligibly small. In practice, this term can be ignored in comparison with other uncertainties, as shown in the Appendix. The calculated result presented below is considered accurate, but it is subject to possible errors in the above assumptions. Our purpose for calculating the antenna pattern corrections is to give an estimate of the magnitude of the effects of the sidelobes. Data users, who want more accurate results, should perform their own calculations, using the $\overline{T}_E$ and $\overline{T}_{\rm Sat}$ values, which may be more appropriate to the actual environmental conditions at the data collection time and locations.

Main beam efficiency is another important characteristic of the antenna pattern function. It is defined as the ratio of the power received within the main beamwidth to the total power from all angles collected by the antenna system, including both copolarized and cross-polarized power. Here, the main beamwidth is defined as 2.5× the measured 3-dB beamwidth of an antenna pattern. Practically, the main beam efficiency can be calculated from (14) by replacing the integration limit with a half-cone angle equal to 1.25× the 3-dB beamwidth. This is defined as

$$f_{\rm main}(\beta) = \frac{1}{N}\int_0^{\theta_{\rm main}} g(\theta)\,\sin\theta\,d\theta \quad (15)$$

where $\theta_{\rm main}$ equals 1.25× the 3-dB beamwidth for individual channels, as given in Table I.

III. Description of Antenna Pattern Data

The NOAA-K AMSU-A instrument consists of the AMSU-A2 protoflight model (PFM) and AMSU-A1 flight model 1 (FM1). Antenna pattern data for both models were measured by Aerojet, the instrument's manufacturer. Detailed description of the data measurement process was given elsewhere [9]. Only a brief description of the measurements is described here.

The antenna pattern data were measured at each channel frequency, except channels 9–14, which share the same central frequency (57.29 GHz). Therefore, the antenna pattern data used in this study consist of ten channels with different central frequencies. The measurements were performed at the intermediate frequency (IF) outputs of the mixer/amplifiers. A spectrum analyzer was used to accommodate testing at the IF outputs of the instrument. To achieve the required 55-dB dynamic range for these measurements, the patterns were measured in two parts: 1) in the main beam region, a 20 dB of attenuation was inserted in the range transmitter and 2) in the sidelobe region, the attenuation was removed. The measurement process starts with the operator positioning the antenna at the peak of the beam with 20 dB of attenuation inserted before the transmit horn of the measurement system, at which point he or she begins the test on the antenna range controller that measures the power received at this point and sets this power level to the top of the scale on the spectrum analyzer. The controller then moves the antenna positioner and measures the antenna pattern for an angular span of 10° centered on the peak of the beam with an increment size of 0.2°. The angular span of 10° was selected because it covers the 20–30-dB range of the central antenna pattern. The data were digitally recorded and read from the spectrum analyzer. At the second step of the measurement, the 20-dB attenuator is removed and the antenna pattern over the other angular span is measured. The controller measures the power level received from the spectrum analyzer at each measurement and subtracts 20 dB from this reading and stores the results. At each of these ten channel frequencies, the measured data consist of elements, as follows.

- Four planes: At each frequency, antenna pattern data were measured at four plane "cuts." Each cut corresponds to two azimuthal angles, i.e., $\gamma = 0$ and 180, 45 and 225, 90 and 270, and 135 and 315°, respectively. These plane cuts will be referred to as the 0, 45, 90, and 135 cuts, respectively.
- Angular range and scan interval: The scanning angle (i.e., α) extends from 0 to ±180° from the antenna boresight with 0.2° steps.
- Fine-step data: For accurate determination of the antenna beamwidths, the central parts of the antenna pattern (0 to ±4.5°) were measured at steps of 0.05°. These fine-step data were measured at two plane cuts, crosstrack ($\gamma = 0°$) and downtrack ($\gamma = 90°$) cuts, respectively.
- Three beam positions: Data were taken at three earth viewing beam positions, 1, 15, and 30, respectively.
- Two polarizations: Each set of these antenna patterns was measured with two different polarizations (copolarizations and cross polarizations).

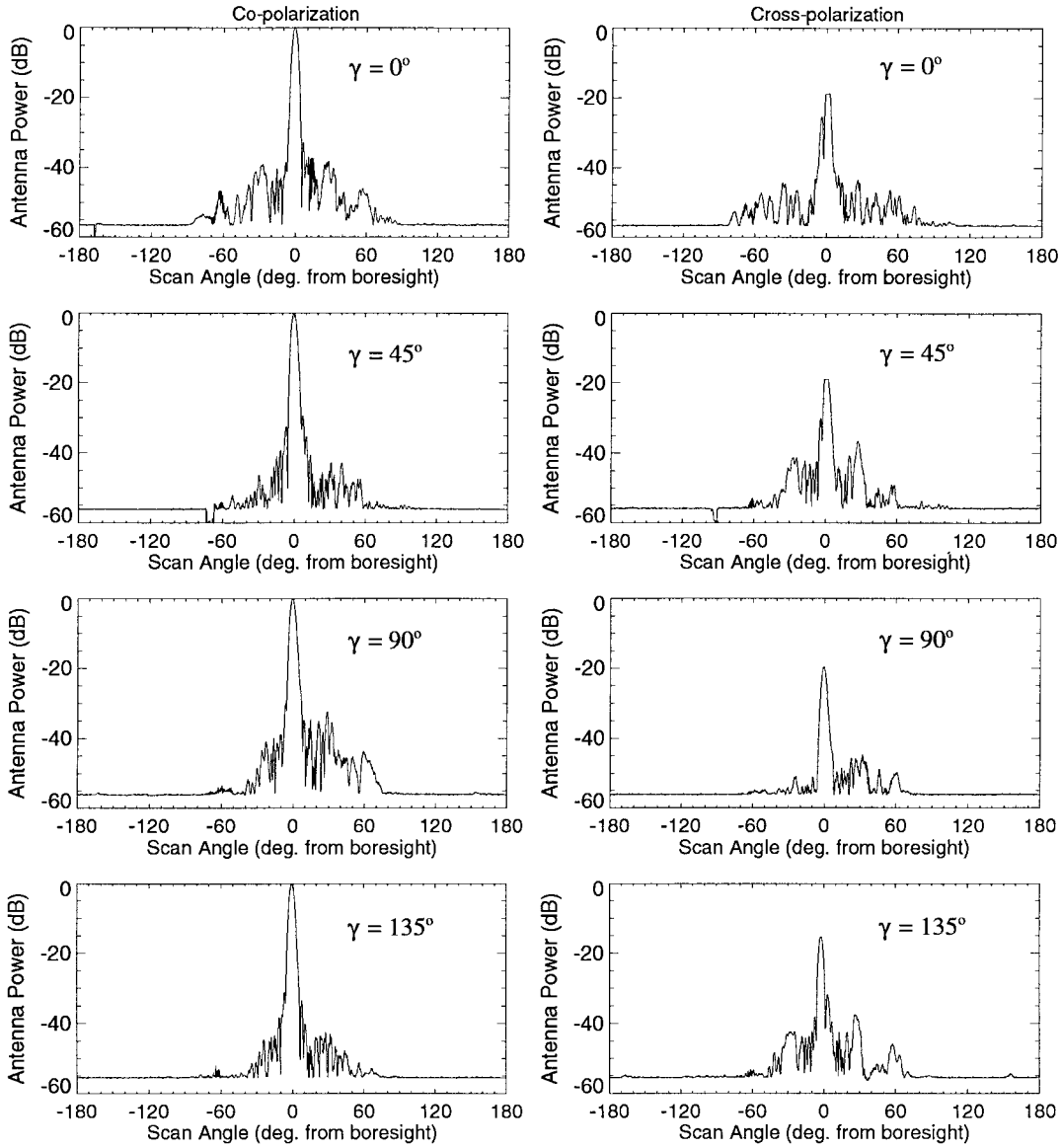

Fig. 2. Sample of antenna pattern data from AMSU-A FM1 channel 3 (50.3 GHz). The left-hand column contains the copolarization data, while cross-polarization data are displayed in the right-hand column. The 0, 45, 90, and 135° cuts are displayed from top to bottom. For each cut, both copolarized and cross-polarized data were normalized relative to the boresight peak of copolarization.

Fig. 2 shows a sample of the antenna pattern data, which were measured at the frequency of 50.3 GHz (channel 3) at the beam position 15 for all four cuts. The 0° cut corresponds to the crosstrack scan plane, while the 90° cut is in the downtrack plane. At each cut, the central peak of the copolarization power was normalized to 0 dB, to which all other data points were scaled. The copolarization data are shown in the left-hand column, while the cross polarizations are displayed in right-hand column. Results in Fig. 2 show that the cross-polarization spectra are approximately 20 dB smaller than the corresponding ones in copolarization in the main lobe. However, the cross- and copolarized power signals in the sidelobes at large scan angles have about the same magnitudes.

IV. Results

The formulas developed in Section II were used to generate the results described in this section. The antenna pattern data described above were also used to calculate the 3-dB beamwidths and the main beam efficiencies. Calculations of antenna efficiencies over three different solid-angle regions subtended at the satellite by the earth (plus atmosphere below 20 km), cold space, and the satellite platform are performed at 30 earth views and four cold space views. Errors associated with the uncertainty in the antenna pattern measurements are presented in the Appendix. These calculated antenna efficiencies were then used to simulate the AMSU-A antenna temperatures.

A. Beamwidths

The 3-dB beamwidth is defined as the full angular width between two angles, in which the magnitude of antenna pattern drops to one-half of its peak value at boresight. The fine-step antenna data were used in determination of individual channel 3-dB beamwidths. Linear interpolation of the fine-step data was used to determine the exact half-power locations. Table I lists these measured 3-dB beamwidths at beam position

TABLE II
NOAA-K AMSU-A ANTENNA EFFICIENCIES OVER REGIONS OF EARTH, SATELLITE PLATFORM, AND COLD SPACE. THE SCAN ANGLE IS IN DEGREES

Beam Postion	Scan Angle	Ch. 1			Ch. 2			Ch. 3			Ch. 4			Ch. 5		
	β	fe (%)	fsat (%)	fc (%)	fe (%)	fsat (%)	fc (%)	fe (%)	fsat (%)	fc (%)	fe (%)	fsat (%)	fc (%)	fe (%)	fsat (%)	fc (%)
1	48.33	98.70	0.37	0.93	99.38	0.19	0.42	98.54	0.67	0.79	98.89	0.27	0.84	98.81	0.31	0.88
3	41.67	98.89	0.31	0.80	99.46	0.17	0.37	98.66	0.67	0.67	99.09	0.23	0.68	99.01	0.28	0.71
5	35.00	99.07	0.26	0.67	99.53	0.15	0.32	98.81	0.65	0.54	99.34	0.21	0.46	99.26	0.25	0.49
7	28.33	99.15	0.22	0.63	99.60	0.13	0.28	98.90	0.63	0.48	99.48	0.19	0.33	99.43	0.23	0.34
9	21.67	99.25	0.18	0.56	99.65	0.11	0.24	98.92	0.63	0.46	99.52	0.19	0.29	99.45	0.22	0.33
11	15.00	99.32	0.16	0.52	99.66	0.11	0.23	98.92	0.63	0.45	99.56	0.19	0.25	99.46	0.21	0.33
13	8.33	99.36	0.16	0.49	99.66	0.11	0.23	98.92	0.64	0.44	99.59	0.19	0.22	99.48	0.21	0.31
15	1.67	99.41	0.16	0.44	99.66	0.11	0.23	98.92	0.66	0.42	99.60	0.19	0.21	99.48	0.22	0.30
16	-1.67	99.43	0.15	0.42	99.67	0.11	0.22	98.91	0.66	0.43	99.60	0.19	0.21	99.48	0.22	0.30
18	-8.33	99.42	0.14	0.44	99.66	0.11	0.23	98.88	0.66	0.46	99.59	0.19	0.22	99.45	0.22	0.33
20	-15.00	99.37	0.14	0.49	99.63	0.11	0.26	98.86	0.66	0.48	99.57	0.20	0.23	99.43	0.22	0.35
22	-21.67	99.29	0.15	0.56	99.58	0.12	0.30	98.83	0.67	0.50	99.53	0.20	0.27	99.40	0.23	0.36
24	-28.33	99.11	0.15	0.74	99.49	0.14	0.37	98.77	0.69	0.54	99.48	0.21	0.31	99.36	0.24	0.39
26	-35.00	98.92	0.18	0.90	99.40	0.17	0.44	98.65	0.71	0.64	99.33	0.23	0.44	99.20	0.28	0.52
28	-41.67	98.68	0.23	1.09	99.30	0.20	0.49	98.46	0.75	0.79	99.13	0.24	0.63	98.98	0.31	0.71
30	-48.33	98.51	0.29	1.20	99.22	0.25	0.53	98.32	0.78	0.91	98.95	0.28	0.77	98.76	0.34	0.89
CC 4	-76.67	0.91	1.17	97.92	0.48	0.67	98.85	0.92	1.26	97.82	0.82	0.82	98.37	0.86	1.00	98.14
CC 3	-80.00	0.81	1.28	97.91	0.43	0.72	98.85	0.84	1.35	97.81	0.71	0.91	98.38	0.75	1.16	98.09
CC 2	-81.67	0.76	1.34	97.90	0.40	0.74	98.86	0.81	1.40	97.79	0.66	0.97	98.37	0.70	1.23	98.07
CC 1	-83.33	0.70	1.39	97.91	0.36	0.78	98.86	0.78	1.46	97.76	0.61	1.05	98.34	0.65	1.31	98.04

Beam Postion	Scan Angle	Ch. 6			Ch. 7			Ch. 8			Ch. 9 - 14			Ch. 15		
	β	fe (%)	fsat (%)	fc (%)	fe (%)	fsat (%)	fc (%)	fe (%)	fsat (%)	fc (%)	fe (%)	fsat (%)	fc (%)	fe (%)	fsat (%)	fc (%)
1	48.33	99.16	0.20	0.65	98.82	0.25	0.94	98.72	0.44	0.84	99.33	0.21	0.46	99.51	0.24	0.25
3	41.67	99.33	0.17	0.50	99.00	0.20	0.81	98.91	0.41	0.68	99.43	0.19	0.38	99.56	0.22	0.22
5	35.00	99.51	0.14	0.35	99.21	0.16	0.63	99.12	0.39	0.48	99.54	0.17	0.29	99.58	0.23	0.19
7	28.33	99.63	0.12	0.24	99.35	0.15	0.50	99.26	0.39	0.35	99.61	0.16	0.23	99.60	0.22	0.18
9	21.67	99.68	0.11	0.21	99.41	0.14	0.45	99.29	0.39	0.33	99.65	0.15	0.20	99.60	0.23	0.17
11	15.00	99.71	0.10	0.19	99.48	0.13	0.38	99.32	0.39	0.29	99.67	0.14	0.19	99.60	0.23	0.17
13	8.33	99.74	0.10	0.17	99.52	0.13	0.35	99.32	0.40	0.29	99.68	0.14	0.17	99.59	0.24	0.17
15	1.67	99.75	0.10	0.15	99.53	0.13	0.33	99.30	0.40	0.29	99.69	0.15	0.16	99.58	0.24	0.18
16	-1.67	99.77	0.10	0.14	99.53	0.13	0.33	99.29	0.41	0.31	99.71	0.15	0.14	99.58	0.24	0.18
18	-8.33	99.77	0.09	0.13	99.54	0.13	0.33	99.29	0.40	0.31	99.72	0.15	0.14	99.58	0.24	0.17
20	-15.00	99.76	0.09	0.15	99.47	0.13	0.40	99.28	0.40	0.32	99.71	0.15	0.15	99.59	0.24	0.17
22	-21.67	99.73	0.09	0.17	99.37	0.13	0.50	99.24	0.41	0.35	99.69	0.15	0.17	99.58	0.24	0.18
24	-28.33	99.68	0.09	0.23	99.27	0.13	0.59	99.21	0.43	0.37	99.65	0.15	0.21	99.58	0.24	0.18
26	-35.00	99.53	0.10	0.37	99.11	0.14	0.75	99.10	0.44	0.46	99.57	0.15	0.28	99.55	0.24	0.21
28	-41.67	99.34	0.12	0.54	98.87	0.19	0.94	98.84	0.46	0.70	99.44	0.16	0.40	99.51	0.24	0.25
30	-48.33	99.19	0.14	0.67	98.64	0.26	1.11	98.60	0.49	0.91	99.32	0.18	0.51	99.44	0.25	0.31
CC 4	-76.67	0.68	0.69	98.63	0.61	0.93	98.46	0.87	1.09	98.03	0.45	0.52	99.02	0.24	0.40	99.36
CC 3	-80.00	0.57	0.83	98.60	0.55	1.08	98.36	0.76	1.24	98.00	0.40	0.63	98.97	0.23	0.43	99.35
CC 2	-81.67	0.54	0.91	98.55	0.53	1.16	98.31	0.71	1.31	97.98	0.38	0.71	98.91	0.22	0.44	99.34
CC 1	-83.33	0.49	0.99	98.51	0.50	1.26	98.24	0.65	1.38	97.96	0.36	0.78	98.85	0.21	0.46	99.33

Note: CC = Cold Calibration Position

15 for all channels, except channels 10–14, which share the same central frequency as channel 9. No measurement of antenna pattern was made for these channels. We assume that the 3-dB beamwidths for channels 10–14 are the same as that of channel 9. The channel central frequencies are also listed in Table I. Each of the 3-dB beamwidths in Table I is the average value of those obtained from the crosstrack and downtrack measurements of antenna pattern data in fine steps. Differences between the crosstrack and downtrack 3-dB beamwidths are insignificant. It is shown in the Appendix that these beamwidths have standard deviations $\leq 0.01°$.

AMSU-A specification requires $3.3° \pm 10\%$ for the 3-dB beamwidths. Table I shows that the beamwidths at channels 3–6 and 15 exceed the $3.3° \pm 10\%$ (i.e., 2.97–3.63°) specification. The largest deviation occurs at channel 15 with measured value of 3.80°. Therefore, the surface resolution cells for these channels will increase proportionally.

B. Main Beam Efficiencies

The main beam efficiency is defined in (15) with θ_{main} equal to $1.25\times$ the 3-dB beamwidth at each channel. Using the 3-dB beamwidths in Table I, we calculated the main beam efficiencies for the channels of which measured antenna patterns are available. Also calculated are the cross-polarization beam efficiencies, which are defined as the ratio of the power due to cross polarization only within the main beam to the total power that includes both copolarizations and cross polarizations from all angles. The calculated results (for beam position 15) are listed in Table I. Standard deviations for these beam efficiencies are estimated in the Appendix.

AMSU-A specification requires that the main beam efficiencies should be $\geq$95% for all channels. The results in Table I meet the specification, except channel 7, which is only slightly below the 95% requirement.

C. Antenna Efficiencies over Earth, Cold Space, and Satellite Platform

The antenna efficiencies integrated over the earth (plus 20-km atmosphere), cold space, and satellite platform were calculated from (14). Parts of the calculated results of the three antenna efficiencies $f_e(\beta)$, $f_c(\beta)$, and $f_{\text{sat}}(\beta)$ are listed in Table II for 16 earth viewing positions and four cold sky calibration positions. Values of the other 14 earth viewing positions can be interpolated from those listed in Table II.

TABLE III
η VALUES IN (12)

Channel	f_{Asat} (%)	f_{sat} (%)	$\eta = f_{Asat}/f_{sat}$
1	0.02	1.39	0.01
2	0.06	0.78	0.08
3	0.04	1.46	0.03
4	0.04	1.05	0.04
5	0.05	1.31	0.04
6	0.03	0.99	0.03
7	0.04	1.26	0.03
8	0.06	1.38	0.04
9-14	0.03	0.78	0.04
15	0.05	0.46	0.11

The $f_{\rm sat}$ values (Table II) at the cold calibration positions are in the order of 1% without including the near-field effect of the satellite platform. During the calibration process, Aerojet [8] performed a computer simulation of this near-field effect on the antenna efficiency and calculated one set of the $f_{\rm sat}$ values at the cold calibration position CC1 for individual channels. These calculated results are listed in Table III in the second column, which is labeled as $f_{\rm Asat}$. For comparison, the corresponding $f_{\rm sat}$ values at CC1 from Table II are taken and listed in the third column in Table III. We can see that the near-field effect reduces the contribution from the satellite platform. To reduce the $f_{\rm sat}$ values to the same magnitude as those of the computer-simulated results, we define the scale factor η, which appears in (12) as

$$\eta = \frac{f_{\rm Asat}}{f_{\rm sat}}. \tag{16}$$

The η values for all channels are listed in the last column in Table III. These η values will be used in computing the antenna temperatures from (12).

D. Antenna Pattern Corrections

The calculated antenna efficiencies in Table II make it easy to perform any antenna pattern sidelobe correction. It has been shown that differences do occur between the true brightness temperatures and antenna temperatures observed by spaceborne radiometers [3]–[6]. There are two main corrections that can be made with the efficiencies in Table II. The first one is that the measurements from earth views are contaminated by radiations originated from the cold space and satellite platform. Similarly, measurements from the cold space views are contaminated by radiations from the earth limbs and satellite platform. Table II shows that the antenna efficiencies over cold space can be about 1% at the edge of earth views. In viewing the earth scenes, this will reduce the observed antenna temperature by about the same percentages below the true brightness temperatures since the microwave cosmic background temperature $\overline{T}_C = 2.73$ K is much smaller than the earth's brightness temperature $\overline{T}_E$. In viewing cold space, the contamination introduced by the earth limb can be up to 0.9%, as shown in Table II. This will produce an effective cold space calibration temperature higher than the nominal value of $\overline{T}_C = 2.73$ K.

As discussed in Section II, the quantity $\overline{T}_{\rm Sat}$, which represents the total energy emanation associated with the satellite platform, may consist of satellite-platform radiation as well as reflection of radiations from the earth and cold space. In practice, it is difficult (if it is not impossible) to select a single $\overline{T}_{\rm Sat}$ value for representing these radiation sources. However, the maximum limit due to this $\overline{T}_{\rm Sat}$ contribution to (12) is only approximately 0.01 K in magnitude, which is obtained by assuming that the whole $\overline{T}_{\rm Sat}$ contribution is attributable to radiation from the satellite platform at an operational spacecraft temperature $\sim$280 K, which is higher than the radiation from either earth or cold space. For example, Tables II and III list the values of $f_{\rm sat}$ and η for channel 1 at the beam position 1 as $f_{\rm sat} = 0.0037$ and $\eta = 0.01$; therefore, substituting these values into the last term in (12), we obtain $\Delta T{\rm sat} = (f_{\rm sat}\eta\overline{T}_{\rm Sat})/N_\eta = 0.01$ K. Inclusion of reflection of radiation from earth or cold space will reduce the magnitude even smaller than 0.01 K. A reasonable estimate is that approximately half of the upper hemisphere (which subtends 2π steradian of solid angle) may receive cold space radiation reflected from the sides of the satellite platform. Then the above $\Delta T{\rm sat}$ value would be further reduced under such assumption. This shows that the contribution from the last term in (12) is negligibly small, particularly, in comparison to other uncertainties, as discussed in the Appendix. Nevertheless, we retain this term with the knowledge that its effect on the final results is negligible.

To demonstrate the effect of the antenna pattern sidelobes on the antenna temperatures, we apply (12) to calculate a set of antenna temperatures, T_A, at the earth scenes, using the calculated antenna efficiencies (Table II), η values (Table III), and a set of atmospheric brightness temperature profiles that corresponds to an approximate estimate of AMSU-A measurements. Then, the antenna pattern corrections (of the earth views), which are defined as $\Delta T = T_B - T_A$, are calculated. These calculated ΔT results are shown in Fig. 3, which shows that channel 1 has the largest ΔT and that the smallest ΔT occurs at channel 15. Similarly, the antenna pattern corrections at the space views, $\Delta T_C = 2.73$ K $-T_A$, were also calculated and the results are shown in Fig. 4, which shows calibration position 1 (CC1) has the least contamination. Possible errors due to measurement uncertainty in antenna patterns are described in the Appendix.

The $\overline{T}_E$ values used in this simulation are 230 K for channels 1–4 and 15, 240 K for channel 5, and 210 K for channels 6–9, respectively. For the four cold space calibration positions, $\overline{T}_E = 210$ K were used to calculate the antenna temperatures (see discussion in Section II). The ΔT values in Fig. 3 correspond to fixed biases in the antenna system and should be incorporated into the antenna temperatures to obtain the true brightness temperatures. Similarly, the ΔT_C values in Fig. 4 should be combined with T_C (=2.73) K to obtain a set of "effective" cold calibration temperatures. After launch, the in-orbit data will be analyzed to verify these predicted values.

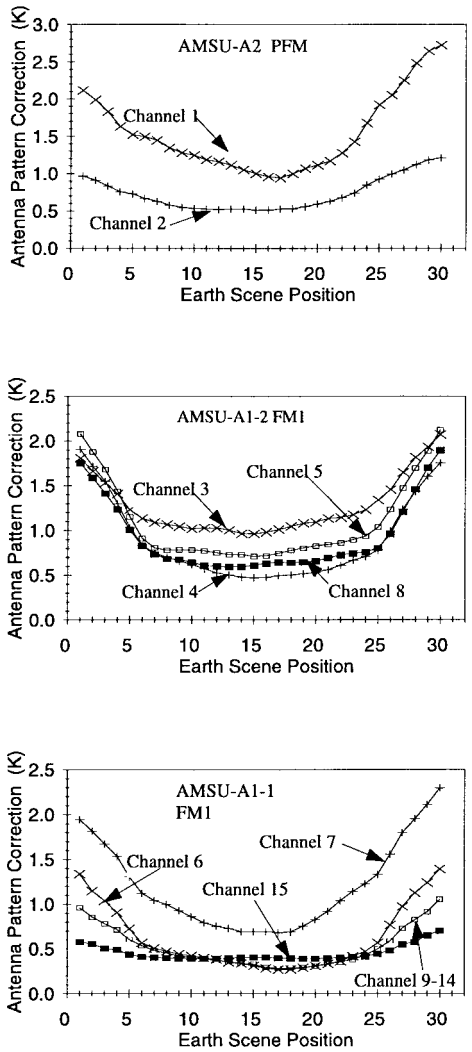

Fig. 3. Sample of calculated antenna pattern corrections, $\Delta T = T_B - T_A$, as described in the text.

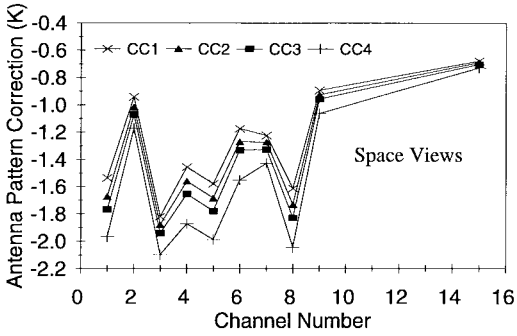

Fig. 4. Calculated antenna pattern corrections $\Delta T_C = 2.73K - T_A$ for the four space views. Note that calculations were done in radiances, which were converted into temperatures, as shown here.

V. Conclusion

This study provides detailed information about the measured antenna pattern data from the NOAA-K AMSU-A instruments and presents a procedure for performing antenna pattern sidelobe corrections to antenna temperatures. The 3-dB beamwidths and main beam efficiencies were also calculated from the antenna pattern data for comparison with the AMSU-A specifications of 95% (or better) for the main beam efficiencies and 3.3° ± 10% for the 3-dB beamwidths.

Predictions of antenna pattern sidelobe corrections were made over three solid-angle regions subtended at the satellite by the earth (plus 20-km atmosphere), cold space, and the satellite platform. Antenna efficiencies over these three solid-angle regions were presented at 16 earth views and four possible cold space calibration views of the AMSU-A scan operation. These calculated antenna efficiencies make it possible to perform antenna pattern sidelobe corrections. A sample simulation using these antenna efficiencies and a profile of atmospheric brightness temperatures shows that the resultant antenna pattern corrections can be more than 2 K (Fig. 3) for some channel fields of view on the edges of scan swath, in which more cold space radiance is sensed via the antenna side lobes.

Calculation shows that the contribution from the satellite platform [the last term in (12)] is negligibly small, with a magnitude less than 0.01 K, which can be ignored in comparison to other uncertainties, as discussed in the Appendix.

Computations of the antenna pattern corrections at the four possible cold space calibration positions reveal that the space view CC1 for all channels has the least contamination from the earth and satellite platform. We should note that an optimal choice of the cold space views will be made after launch of AMSU-A and these antenna pattern corrections will be compared to those obtained using the in-orbit data during the instrument's activation and evaluation period.

The antenna efficiencies presented in this study make it easy to design an algorithm for performing antenna pattern corrections to the antenna temperatures from the AMSU-A data.

Note Added in Proof: On May 13, 1998, the NOAA-K, which has now been designated NOAA-15, was successfully launched into a circular, near-polar orbit with an alititude of 833 km above the earth and an inclination angle of 98.7° to the equator. All channels on the NOAA-15 AMSU-A have performed well since its powering up after launch.

Appendix
Antenna Pattern Measurement Errors

The far-field antenna pattern measurement accuracy (or error) is estimated from the amplitude error analysis techniques. Beside the antenna pattern measurements, Aerojet measured the antenna noise level of power signals reflected (or scattered) from the sides of the antenna test chamber. Although we do not know the phase of this reflected signal relative to the direct path, these noise level signals can be used for calculation of the in-phase and out-of-phase fractions [9] of the antenna efficiencies over various solid-angle regions as the upper and lower bounds on the measurement accuracy. The process for calculating the in-phase and out-of-phase errors is outlined as follows:

A. In-Phase Constructive Combination of Antenna Pattern and Noise Signal

For the in-phase case, the antenna pattern in (3) is replaced by an effective antenna pattern G', which is defined as

$$G'(\Omega, \beta) = \left|\sqrt{G_{\rm co}} + \sqrt{G_n}\right|^2 + \left|\sqrt{G_{\rm cross}} + \sqrt{G_n}\right|^2 \quad \text{(A1)}$$

TABLE IV
SAMPLES OF IN-PHASE, OUT-OF-PHASE, AND STANDARD DEVIATION CALCULATIONS OF ANTENNA PATTERN CORRECTIONS

Beam Postion	Scan Angle β (deg.)	ΔT = Tb - Ta IN-PHASE Ch. 1 (K)	Ch. 5 (K)	Ch. 15 (K)	OUT-OF-PHASE Ch. 1 (K)	Ch. 5 (K)	Ch. 15 (K)	Standard Deviation σ Ch. 1 (K)	Ch. 5 (K)	Ch. 15 (K)
1	48.33	3.81	2.93	0.68	1.31	1.64	0.47	0.72	0.37	0.06
3	41.67	3.49	2.48	0.60	1.08	1.26	0.40	0.69	0.35	0.06
5	35.00	3.12	1.89	0.53	0.85	0.77	0.33	0.66	0.32	0.06
7	28.33	3.06	1.50	0.50	0.78	0.44	0.30	0.66	0.31	0.06
9	21.67	2.89	1.48	0.49	0.65	0.42	0.29	0.65	0.31	0.06
11	15.00	2.80	1.48	0.48	0.58	0.40	0.29	0.64	0.31	0.06
13	8.33	2.74	1.45	0.49	0.53	0.36	0.29	0.64	0.32	0.06
15	1.67	2.61	1.43	0.51	0.47	0.33	0.30	0.62	0.32	0.06
16	-1.67	2.56	1.45	0.50	0.44	0.34	0.30	0.61	0.32	0.06
18	-8.33	2.61	1.52	0.49	0.47	0.38	0.29	0.62	0.33	0.06
20	-15.00	2.78	1.59	0.49	0.52	0.42	0.28	0.65	0.34	0.06
22	-21.67	3.01	1.63	0.50	0.61	0.45	0.29	0.69	0.34	0.06
24	-28.33	3.53	1.73	0.52	0.89	0.51	0.31	0.76	0.35	0.06
26	-35.00	3.98	2.07	0.59	1.17	0.79	0.37	0.81	0.37	0.06
28	-41.67	4.51	2.60	0.68	1.50	1.21	0.45	0.87	0.40	0.07
30	-48.33	4.80	3.09	0.83	1.69	1.61	0.57	0.90	0.43	0.07
		ΔT = 2.73 K - Ta								
CC4	-76.67	-4.11	-2.90	-0.92	-1.02	-1.39	-0.56	0.89	0.44	0.10
CC3	-80.00	-3.84	-2.66	-0.89	-0.90	-1.21	-0.54	0.85	0.42	0.10
CC2	-81.67	-3.71	-2.55	-0.88	-0.85	-1.13	-0.52	0.83	0.41	0.10
CC1	-83.33	-3.52	-2.43	-0.87	-0.75	-1.04	-0.51	0.80	0.40	0.10

Note: CC = Cold Calibration Position

where G_n represents the measured antenna noise level power signal reflected from the sides of the antenna test chamber.

B. Out-of-Phase Destructive Combination of Antenna Pattern and Noise Signal

For the out-of-phase case, the antenna pattern in (3) is replaced by an effective antenna pattern G'', which is defined as

$$G''(\Omega, \beta) = \left|\sqrt{G_{\rm co}} - \sqrt{G_n}\right|^2 + \left|\sqrt{G_{\rm cross}} - \sqrt{G_n}\right|^2. \quad \text{(A2)}$$

The measured G_n values supplied by Aerojet are $G_n = -57.3$ dB for channel 2 (31.4 GHz), -63 dB for channels 3–9, and -74.5 dB for channel 15. No measurement for channel 1 (23.8 GHz) was available, but we assume that its G_n is the same as that channel 2. Using these G_n values, we calculated the in-phase and out-of-phase antenna efficiencies f_e, $f_{\rm sat}$, and f_c, respectively. The results are similar to those in Table II. From these in-phase and out-of-phase antenna pattern efficiencies, we calculated the corresponding in-phase and out-phase antenna pattern corrections ΔT, similar to those shown in Figs. 3 and 4. Table IV lists some samples (for channels 1, 5, and 15) of the calculated in-phase and out-of-phase antenna pattern corrections, which correspond to the maximum and minimum possible corrections, respectively, to the antenna temperatures.

Results in Table IV show that the magnitudes of antenna pattern corrections are quite different for the in-phase and out-of-phase cases. This implies that it is very important to accurately determine the G_n values in any antenna pattern measurement.

From the maximum and minimum antenna pattern corrections in Table IV, we can compute the standard deviation σ of the antenna pattern corrections. We assume that the distribution of errors is uniform between the maximum (in-phase) and minimum (out-of-phase) antenna pattern corrections in Table IV. This uniform probability distribution function can be represented by

$$\begin{aligned} f(x) &= \frac{1}{T_{\rm max} - T_{\rm min}}, && \text{if } T_{\rm min} \le x \le T_{\rm max} \\ &= 0, && \text{if } x < T_{\rm min} \text{ or } x > T_{\rm max} \end{aligned} \quad \text{(A3)}$$

where $T_{\rm max}$ and $T_{\rm min}$ represent the in-phase and out-of phase calculated antenna pattern corrections, respectively. The standard deviation is defined as

$$\sigma = \sqrt{\int_{T_{\rm min}}^{T_{\rm max}} f(x)(x - \overline{x})^2\, dx} \quad \text{(A4)}$$

where $\overline{x} = (T_{\rm max} + T_{\rm min})$ is the mean of the maximum and minimum antenna pattern corrections. The calculated σ values for the three channels are listed in the last three columns in Table IV. These σ values represent an upper limit of uncertainty for the antenna pattern corrections as shown in Figs. 3 and 4.

Similarly, the accuracies for the beamwidths and beam efficiencies in Table I can be estimated by the same method as presented above. The standard deviations for these quantities were calculated and sample results for channels 1, 5, and 15 are listed in Table V.

TABLE V
SAMPLES OF CALCULATED STANDARD DEVIATIONS FOR THE BEAMWIDTHS, BEAM EFFICIENCIES, AS LISTED IN TABLE I

Channel Number	Standard Deviation for Beamwidth (deg.)	Main Beam Efficiency	Cross Polarization Beam Efficiency
1	0.009	0.090%	0.015%
5	0.005	0.003%	0.000%
15	0.001	0.003%	0.000%

ACKNOWLEDGMENT

Aerojet is the primary contractor for building the AMSU-A instruments and measured antenna patterns used in this study. The author gratefully acknowledges the helpful comments and discussions made by Dr. L. Crone, NOAA/NESDIS, during this study. The author also wishes to thank Dr. P. Rosenkranz, Massachusetts Institute of Technology, for his helpful comments on the interpretation of the near-field issue and estimate of the antenna measurement errors as well as Dr. J. Shiue, NASA/Goddard Space Flight Center, for many discussions about the antenna systems. Comments and suggestions by three anonymous reviewers resulted in improving the manuscript.

REFERENCES

[1] T. Mo, "Prelaunch calibration of the advanced microwave sounding unit-A for NOAA-K," *IEEE Trans. Microwave Theory Tech.*, vol. 44, pp. 1460–1469, Dec. 1996.

[2] R. W. Rogers, T. J. Hewison, N. C. Atkinson, and S. J. Stringer, "The radiometric characterization of AMSU-B," *IEEE Trans. Microwave Theory Tech.*, vol. 43, pp. 760–771, May 1995.

[3] J. P. Classen and A. K. Fung, "The recovery of polarized apparent temperature distributions of flat scenes from antenna temperature measurements," *IEEE Trans. Antennas Propagat.*, vol. AP-22, pp. 433–442, May 1974.

[4] E. G. Njoku, "Antenna pattern correction procedures for the scanning multichannel microwave radiometer (SMMR)," *Boundary Layer Meteorol.*, vol. 18, pp. 79–98, 1980.

[5] N. Grody, "Antenna temperature for a scanning microwave radiometer," *IEEE Trans. Antennas Propagat.*, vol. AP-28, pp. 141–144, Jan. 1975.

[6] T. J. Hewsion and R. Saunders, "Measurements of the AMSU-B antenna pattern," *IEEE Trans. Geosci. Remote Sensing*, vol. 34, pp. 405–412, Mar. 1996.

[7] D. Brest, GenCorp Aerojet, Azusa, CA, 1997, private communication.

[8] "Calibration log book for AMSU-A," Aerojet, Azusa, CA, Rep. 10481A, Sept. 1996.

[9] "AMSU-A Verification Test Report," Aerojet, Azusa, CA, Rep. 9875-3A, June 1994.

Tsan Mo received the Ph.D. degree in physics from the University of Maryland, College Park.

He has worked in the fields of nuclear physics, atmospheric sciences, and microwave remote sensing. Currently, he is with NOAA/NESDIS, Camp Springs, MD, working on microwave remote sensing and satellite data.